Biogeosciences, 11, 3149–3161, 2014
www.biogeosciences.net/11/3149/2014/
doi:10.5194/bg-11-3149-2014

Biogeosciences Open Access

^{17}O excess traces atmospheric nitrate in paleo-groundwater of the Saharan desert

M. Dietzel[1], A. Leis[2], R. Abdalla[1], J. Savarino[3,4], S. Morin[5], M. E. Böttcher[6,*], and S. Köhler[1,]**

[1]Graz University of Technology, Institute of Applied Geosciences, Rechbauerstrasse 12, 8010 Graz, Austria
[2]Joanneum Research, Institute of Water Resources Management, Graz, Austria
[3]CNRS, LGGE, 38000 Grenoble, France
[4]Univ. Grenoble Alpes, LGGE, 38000 Grenoble, France
[5]Météo-France – CNRS, CNRM-GAME UMR 3589, CEN, Grenoble, France
[6]Biogeochemistry Department, Max Planck Institute for Marine Microbiology, 28359 Bremen, Germany
[*]now at: Leibniz Institute for Baltic Sea Research, Geochemistry & Isotope Geochemistry Group, 18119 Warnemünde, Germany
[**]now at: Department of Aquatic Sciences and Assessment, Swedish University of Agricultural Sciences, Uppsala, Sweden

Correspondence to: M. Dietzel (martin.dietzel@tugraz.at)

Received: 3 October 2013 – Published in Biogeosciences Discuss.: 20 December 2013
Revised: 12 April 2014 – Accepted: 16 April 2014 – Published: 17 June 2014

Abstract. Saharan paleo-groundwater from the Hasouna area of Libya contains up to 1.8 mM of nitrate, which exceeds the World Health Organization limit for drinking water, but the origin is still disputed. Herein we show that a positive ^{17}O excess in NO_3^- ($\Delta^{17}O_{NO_3} = \delta^{17}O_{NO_3} - 0.52\,\delta^{18}O_{NO_3}$) is preserved in the paleo-groundwater. The ^{17}O excess provides an excellent tracer of atmospheric NO_3^-, which is caused by the interaction of ozone with NO_x via photochemical reactions, coupled with a non-mass-dependent isotope fractionation. Our $\Delta^{17}O_{NO_3}$ data from 0.4 to 5.0 ‰ ($n = 28$) indicate that up to 20 mol % of total dissolved NO_3^- originated from the Earth's atmosphere ($x[NO_3^-]_{atm}$), where the remaining NO_3^- refers to microbially induced nitrification in soils. High $\Delta^{17}O_{NO_3}$ values correspond to soils that are barren in dry periods, while low $\Delta^{17}O_{NO_3}$ values correspond to more fertile soils. Coupled high $\Delta^{17}O_{NO_3}$ and high $x[NO_3^-]_{atm}$ values are caused by a sudden wash-out of accumulated disposition of atmospheric NO_3^- on plants, soil surfaces and in vadose zones within humid–wet cycles. The individual isotope and chemical composition of the Hasouna groundwater can be followed by a binary mixing approach using the lowest and highest mineralised groundwater as end members without considering evaporation. Using the $\delta^{34}S_{SO_4}$ and $\delta^{18}O_{SO_4}$ isotope signature of dissolved SO_4^{2-}, no indication is found for a superimposition by denitrification, e.g. involving pyrite minerals within the aquifers. It is suggested that dissolved SO_4^{2-} originates from the dissolution of $CaSO_4$ minerals during groundwater evolution.

1 Introduction

The accumulation of nitrate (NO_3^-) in groundwater is a well-known phenomenon occurring worldwide (Clark and Fritz, 1997; Kendall, 1998). Individual NO_3^- sources and mechanisms for its accumulation depend strongly on the environmental conditions during recharge, infiltration, and aquifer storage. High NO_3^- concentrations of paleo-groundwater from the Hasouna area (Libya) have been measured for decades, but the NO_3^- origin is still hotly debated (El-Baruni et al., 1985; Milne-Home and Sahli, 2007). Deciphering the source of NO_3^- for Saharan groundwater in Libya is highly challenging, as (i) the present arid conditions preclude appreciable recharge and (ii) groundwater is about 90 % of the source of the water supply of Libya (e.g. Salem, 1992; Edmunds, 2006; Abdelrhem et al., 2008). Several million m^3 of fresh water per day are transferred to the Mediterranean for agricultural and domestic use including drinking water supply.

The source of dissolved NO_3^- in groundwater is commonly attributed to (i) anthropogenic origin, including leaching of fertilisers or animal waste, (ii) the dissolution of evaporite deposits, (iii) leaching of organic or inorganic nitrogen from soils, and (iv) atmospheric deposition (e.g. Clark and Fritz, 1997, Saccon et al., 2013, and references therein). Ancient Saharan groundwater of Hasouna (Libya) was recharged under environmental conditions that did not allow for an anthropogenic impact, but natural provenances of dissolved NO_3^- of the paleo-groundwater have not yet been deciphered and quantified.

Evidence for NO_3^- origin is traditionally obtained by measuring $\delta^{15}N_{NO_3}$ and $\delta^{18}O_{NO_3}$ values (Amberger and Schmidt, 1987; Kendall, 1998). From $\delta^{15}N_{NO_3}$ and $\delta^{18}O_{NO_3}$ data, the NO_3^- provenances can be evaluated, and reaction mechanisms like denitrification may be deduced by considering changes in NO_3^- concentration and mass-dependent isotope fractionation (MDF) (Kendall, 1998). For instance, the discrimination of ^{15}N vs. ^{14}N through denitrification will result in an increase in $\delta^{15}N_{NO_3}$ values of the remaining NO_3^-. Accordingly, a trend to higher $\delta^{15}N_{NO_3}$ values at lower NO_3^- concentrations can be found in groundwater due to denitrification. However, throughout complex processes of nitrogen conversion in soils and within the aquifer $\delta^{15}N_{NO_3}$ and $\delta^{18}O_{NO_3}$ values of dissolved NO_3^- can be strongly overprinted (e.g. by (de)nitrification; Xue et al., 2009).

More recently, a triple stable isotope approach using $^{18}O/^{16}O$ and $^{17}O/^{16}O$ signals in NO_3^- was successfully applied to identify exclusively NO_3^- of atmospheric origin. Atmospheric NO_3^- ($NO_{3\,atm}^-$) is characterised by a ^{17}O excess according to the expression

$$\Delta^{17}O_{NO_3} = \delta^{17}O_{NO_3} - 0.52\,\delta^{18}O_{NO_3}, \quad (1)$$

where non-mass-dependent isotope fractionation (NMDF) during the formation of ozone, followed by photochemical reactions between atmospheric NO_x and O_3 to NO_3^-, results in non-zero $\Delta^{17}O_{NO_3}$ values (Michalski et al., 2003; Thiemens, 2006). Böhlke et al. (1997), for instance, found evidence from $\delta^{15}N_{NO_3}$ and $\delta^{18}O_{NO_3}$ analyses for the atmospheric source of NO_3^- for NO_3^--rich salts in the Atacama (Chile) and Mojave (California) deserts. The atmospheric origin of NO_3^- in the Atacama deposits has been confirmed by a pronounced ^{17}O excess (Michalski et al., 2004a). Since then $NO_{3,atm}^-$ has been quantified using the ^{17}O excess for various desert deposits and dissolved NO_3^- in modern groundwater, lakes, and wet depositions (Darrouzet-Nardi et al, 2012; Dejwakh et al., 2012; Li et al., 2010; Michalski et al., 2005; Michalski et al., 2004b; Tsunogai et al., 2011; Tsunogai et al., 2010; Nakagawa et al., 2013).

The aim of the present study is to trace the origin of NO_3^- in Saharan paleo-groundwater by using $\delta^{15}N_{NO_3}$ values and triple stable isotopes of oxygen. This approach has never been used for ancient groundwater, and the major aim of this study is to test the applicability of $\Delta^{17}O_{NO_3}$ values

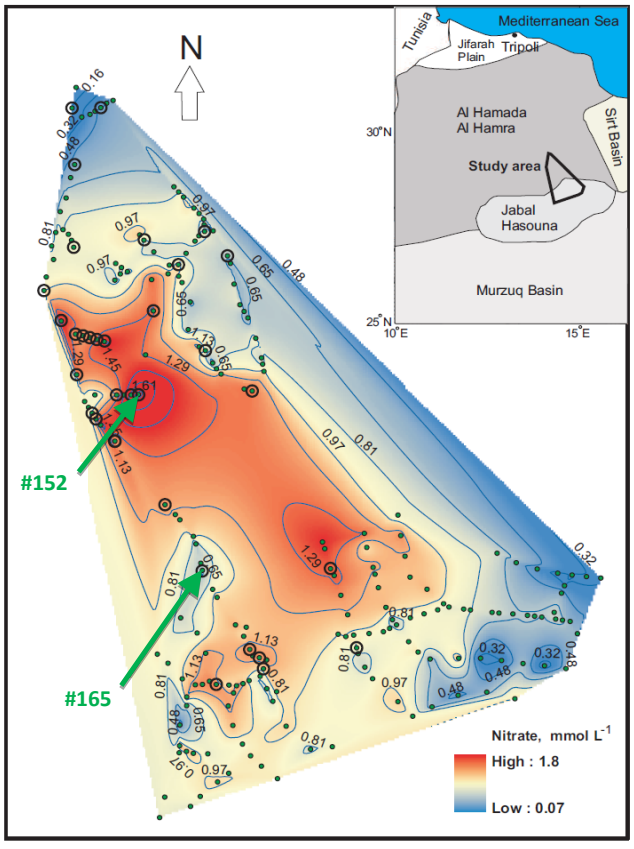

Figure 1. Sampling sites (◯; $n = 28$) and distribution of NO_3^- in paleo-groundwater from Hasouna, Libya. Isolines are obtained from a total of 57 NO_3^- analyses of paleo-groundwater from wells (●).

in such surroundings. In addition, a reaction of NO_3^- with pyrite (FeS_2) minerals in the aquifers can act as a potential NO_3^- sink, which has already been shown for European shallow aquifers (e.g. Böttcher et al., 1990; Zhang et al., 2012). This requires the analyses of the stable isotope signatures of dissolved SO_4^{2-}. Furthermore, ancient recharge and climate conditions are reconstructed by using a multi-element and isotope approach.

2 Study area and sample sites

The Hasouna well field is located about 700 km south of Tripoli (Libya) within the Cambro–Ordovician Nubian Sandstone Aquifer System (Fig. 1). This system comprises one of the world's largest paleo-groundwater aquifers, which had been recharged at approximately 30 ± 10 and 10 ± 3 ka BP based on ^{14}C dating (Edmunds et al., 2003; Edmunds and Wright, 1979; Guendouz et al., 1998; Milne-Home and Sahli, 2007; Sonntag et al., 1978). Strong evidence exists for enhanced precipitation in North Africa during these time periods. However, individual epochs for humidity and groundwater recharge periods are still disputed; Pleistocene and

Holocene humid periods in North Africa have been deduced from the records stored in lacustrine fresh-water sediments (Rognon, 1987), wadi river systems (Kuper and Kröpalin, 2006), travertine (Carrara et al., 1998), paleobotanic investigations (Doherty et al., 2000), rock art dating and varnish coating of petroglyphs (Dietzel et al., 2008), dating of aragonitic mollusk shells (Blackwell et al., 2012), together with cyclicity of geochemical signals observed in marine sediments of the eastern Mediterranean that are influenced by the Nile River hydrology (Wehausen and Brumsack, 1999; Lourens et al., 2001).

The aquifer consists predominantly of fractured sandstone ranging from ≈ 500 to 1500 m in thickness, with thin interbeds of marine limestone and marl. The sandstone itself is mostly quartzitic sandstone, but occasionally carbonate cement occurs. In the study area, the main Cambro–Ordovician sandstone aquifer is overlain by a shallow carbonate aquifer with a basal aquitard, predominantly composed of marly limestone, clay and shale.

Groundwater in the study area of Jabal Hasouna was discovered during oil exploration in the 1960s (Edmunds, 2006). A large number of wells have been installed as part of the Great Man-made River Project, which brings up to ≈ 6 Mm^3 of fresh water per day to the Mediterranean (Salem, 1992; Abdelrhem et al., 2008). The average spacing of the total 484 wells is ≈ 1.5 km, with individual discharges of ≈ 50 $L\,s^{-1}$ covering ≈ 4000 km^2 (Binsariti and Saeed, 2000).

3 Materials and methods

Sampling of Hasouna groundwater from 28 wells was carried out in the year 2007, with sampling depths between 323 and 555 m. Coding and sampling site locations are summarised in Table 1 and shown in Fig. 1.

3.1 Chemical composition

The temperature and pH of the groundwater were measured in situ with pH meter WTW 330 and pH electrode WTW SenTix 41, having a precision of ±0.03 pH units (calibrated on-site using pH 4.0 and 7.0 WTW standard buffer solutions). Concentration of dissolved O_2 was analysed in the field using WTW Oxi 325 and WTW CellOx325, having an analytical precision of ± 0.2 mg L^{-1}. Sampled solutions were filtered in the field through 0.45 µm cellulose acetate membranes, and one aliquot was acidified. The samples were stored in polyethylene and hermetically sealed glass vessels for laboratory analyses. Concentrations of dissolved anions were analysed in non-acidified samples by ion chromatography (Dionex DX 500) with an analytical precision of about ±3 %. Alkalinity was obtained by potentiometric titration of non-acidified samples from the gas-tight glass vessels with an uncertainty of about ±5 %. In the acidified solutions (2 % HNO_3), cations were analysed by inductively coupled optical emission spectroscopy with a precision of better than ±5 % (Perkin Elmer Optima ICP-OES 4300; Merck multi-element standard). Calculation of saturation indices with respect to calcite ($SI_{calcite}$) and gypsum (SI_{gypsum}) was performed with the PHREEQC computer code (Parkhurst and Appelo, 1999) and the phreeqc.dat database.

3.2 Stable isotopes

Additional samples were gathered for analysis of the δD_{H_2O} and $\delta^{18}O_{H_2O}$ values of H_2O. The stable isotopes of hydrogen were measured using a Finnigan DELTA plus XP mass spectrometer working in continuous flow mode by the chromium reduction technique (Morrison et al., 2001). The oxygen isotope composition was measured with a Finnigan DELTA plus mass spectrometer using the classic CO_2–H_2O equilibrium method (Horita et al., 1989). The δD_{H_2O} (analytical precision: ±0.8 ‰) and $\delta^{18}O_{H_2O}$ values (±0.05 ‰) are given relative to the Vienna Standard Mean Ocean Water (VSMOW). As an example, the definition of δ values is given for the D/H distribution in H_2O by the expression

$$\delta D_{H_2O} = (R_s/R_{st} - 1)\ 10^3\ (‰), \quad (2)$$

where R_s and R_{st} are the respective analysed isotope ratios (D/H) for the measured sample and standard (VSMOW), respectively. The $\delta^{34}S_{SO_4}$ and $\delta^{18}O_{SO_4}$ values of dissolved SO_4^{2-} were measured on $BaSO_4$ that was precipitated from acidified solutions by the addition of $Ba(Cl)_2$. The solids were washed and dried and further analysed by means of continuous-flow isotope-ratio monitoring mass spectrometry (CirmMS) using a Thermo Scientific Finnigan Delta+ mass spectrometer at MPI-MM Bremen, Germany (according to Böttcher et al., 2001 and Kornexl et al., 1999). The respective precisions of sulfur and oxygen isotope measurements were ±0.3 ‰ and ±0.5 ‰, for $\delta^{34}S_{SO_4}$ and $\delta^{18}O_{SO_4}$. Results are reported in relation to the VCDT and VSMOW scales, respectively.

Separate samples were taken for isotope analyses of dissolved NO_3^-. Analyses were carried out using the bacterial denitrifier technique in combination with the N_2O decomposition method (Casciotti et al., 2002; Kaiser et al., 2007; Morin et al., 2008; Savarino et al., 2007). Isotope ratios of nitrate were measured on a Thermo Finnigan MAT 253 isotope ratio mass spectrometer, equipped with a GasBench II and coupled to an in-house-built nitrate interface. Briefly, denitrifying Pseudomonas aureofaciens bacteria converts NO_3^- into N_2O under anaerobic conditions. N_2O is then thermally decomposed on a gold surface heated to 900 °C, producing a mixture of O_2 and N_2 which is then separated by gas chromatography and injected into the mass spectrometer for the dual O and N analysis (Erbland et al., 2013, and references therein). Isotopic data were corrected for any isotopic effect occurring during the analytical procedure by using the same approach as Morin et al. (2009) and Frey et al. (2009); international reference materials (IAEA USGS-32, 34 and 35)

Table 1. Composition of Saharan paleo-groundwater from wells of the Hasouna area (Libya). No.: Well number (see Fig. 1). T: Temperature in °C. [ ]: Concentrations are given in mM, except for $O_{2(aq)}$ in mg L^{-1}. Δ_{eq}: Derivation from electrical neutrality in meq %. Site positioning of the wells is given in coordinates X and Y and well depths, D, in metres. $\delta^{18}O_{H_2O}$ and δD_{H_2O} values of the groundwaters are given in ‰ (VSMOW). $\delta^{34}S_{SO_4}$ and $\delta^{18}O_{SO_4}$ values for the isotope composition of dissolved SO_4^{2-} are related to the VCDT and VSMOW standards, respectively, and given in ‰. $\delta^{15}N_{NO_3}$, $\delta^{18}O_{NO_3}$, $\delta^{17}O_{NO_3}$ and $\Delta^{17}O_{NO_3}$ values of the dissolved NO_3^- are given in ‰ relative to the AIR and VSMOW standards, respectively. $x[NO_3^-]_{atm}$: Proportion of dissolved NO_3^- from atmospheric origin with respect to total dissolved NO_3^- in %.

No.	T	pH	$[Ca^{2+}]$	$[Mg^{2+}]$	$[Sr^{2+}]$	$[Na^+]$	$[K^+]$	$[Si(OH)_4]$	$[SO_4^{2-}]$	$[Cl^-]$	$[HCO_3^-]$	$[NO_3^-]$	$[O_{2(aq)}]$	Δ_{meq}	X	Y	D
13	33.0	6.66	2.48	1.33	0.0129	4.23	0.143	0.22	1.63	4.63	3.26	0.54	n.a.	1.5	466 214	3 200 767	535
32	33.2	6.85	2.64	1.30	0.0167	6.64	0.157	0.25	1.77	5.91	3.19	0.76	n.a.	5.0	448 816	3 204 106	499
39	32.7	6.85	2.94	1.49	0.0170	7.42	0.149	0.23	1.83	6.50	3.80	0.95	4.3	5.3	456 039	3 196 409	345
51	29.6	6.74	3.03	1.35	0.0184	9.24	0.149	0.21	2.26	8.43	2.79	0.87	n.a.	4.8	461 602	3 180 497	555
60	30.6	6.54	3.95	1.73	0.0248	12.90	0.171	0.22	2.99	11.21	4.10	1.27	n.a.	4.4	471 372	3 171 846	539
72	33.0	7.12	3.09	1.35	0.0186	8.61	0.136	0.21	2.20	8.71	2.88	1.31	n.a.	1.1	450 790	3 188 993	550
84	35.1	6.79	2.31	1.00	0.0127	5.52	0.136	0.23	1.34	4.43	3.48	0.69	6.5	4.6	434 200	3 202 598	500
89	30.7	7.11	3.63	1.43	0.0200	10.43	0.140	0.24	3.06	8.51	2.71	1.48	5.5	5.2	440 533	3 182 417	453
100	29.9	7.08	2.13	1.19	0.0239	4.57	0.136	0.22	1.50	4.32	3.15	0.69	n.a.	1.1	435 694	3 222 835	500
121	34.4	7.05	3.45	1.41	0.0201	12.57	0.123	0.22	2.63	11.11	3.31	0.81	6.8	4.9	428 000	3 193 342	500
126	30.4	7.18	3.75	1.76	0.0223	13.43	0.146	0.21	3.52	10.74	3.03	1.50	5.4	5.4	431 590	3 186 822	500
134	29.3	6.76	3.25	1.38	0.0192	10.26	0.175	0.21	2.91	7.81	3.00	1.27	4.8	5.3	434 819	3 175 353	500
138	28.9	7.24	2.74	1.06	0.0138	6.67	0.113	0.21	2.14	4.60	3.48	0.88	5.6	4.6	436 464	3 169 606	500
139	28.9	7.46	2.28	0.84	0.0129	4.94	0.091	0.21	1.72	3.78	2.51	0.88	n.a.	3.4	437 292	3 168 351	500
145	29.8	7.00	3.29	2.18	0.0189	9.31	0.128	0.22	2.83	8.13	3.61	1.24	n.a.	4.9	442 758	3 161 113	417
149	28.1	7.40	3.01	1.45	0.0175	8.47	0.133	0.21	2.69	7.60	2.54	1.18	n.a.	2.7	443 135	3 171 020	500
151	28.3	7.00	4.52	2.67	0.0252	13.53	0.173	0.21	3.99	12.25	3.61	1.70	5.7	5.3	446 133	3 171 021	500
152	28.8	7.03	4.51	2.66	0.0275	14.51	0.212	0.24	4.32	13.87	2.51	1.84	5.1	4.4	447 659	3 171 097	500
154	27.2	7.08	3.18	1.50	0.0200	9.95	0.156	0.23	2.93	8.18	3.03	1.18	n.a.	3.6	453 209	3 147 514	524
165	28.1	7.24	2.15	0.63	0.0105	3.47	0.058	0.26	1.53	1.92	2.76	0.59	n.a.	4.8	461 003	3 133 483	500
179	28.1	7.06	3.74	1.10	0.0179	9.57	0.136	0.22	3.20	7.67	3.11	1.20	n.a.	3.0	471 484	3 115 183	343
181	29.7	7.03	3.08	0.91	0.0152	8.89	0.127	0.21	2.86	7.49	2.95	1.02	n.a.	−0.5	473 701	3 112 417	323
286	28.6	7.02	3.34	1.02	0.0168	9.48	0.130	0.22	2.82	7.70	2.87	1.07	n.a.	3.3	474 363	3 114 298	500
372	27.3	7.37	3.37	1.18	0.0207	10.37	0.130	0.24	3.01	8.79	2.79	1.36	n.a.	1.9	488 456	3 132 366	400
384	29.0	7.40	2.69	0.79	0.0151	5.65	0.189	0.24	1.61	4.73	2.98	0.78	n.a.	4.9	493 410	3 115 655	500
442	30.8	7.01	2.39	1.20	0.0150	4.99	0.131	0.22	1.46	4.65	3.23	0.79	n.a.	3.3	460 267	3 205 047	332
453	34.6	6.82	2.15	1.21	0.0131	5.79	0.141	0.24	1.77	4.52	3.87	0.47	n.a.	1.2	439 845	3 232 454	453
478	29.8	7.01	3.06	0.77	0.0225	6.61	0.115	0.22	2.99	5.19	2.36	0.71	n.a.	0.7	463 888	3 109 085	451

No.	$SI_{calcite}$	SI_{gypsum}	$\delta^{18}O_{H_2O}$	δD_{H_2O}	$\delta^{34}S_{SO_4}$	$\delta^{18}O_{SO_4}$	$\delta^{15}N_{NO_3}$	$\delta^{18}O_{NO_3}$	$\delta^{17}O_{NO_3}$	$\Delta^{17}O_{NO_3}$	$x[NO_3^-]_{atm}$
13	−0.50	−1.40	−9.75	−73.2	n.a.	n.a.	9.1	6.9	4.1	0.5	2.0
32	−0.31	−1.37	−9.68	−71.8	n.a.	n.a.	8.4	8.3	6.1	1.8	7.1
39	−0.20	−1.33	−9.72	−72.0	n.a.	n.a.	8.5	13.4	9.5	2.5	10.1
51	−0.49	−1.24	−9.17	−67.6	n.a.	n.a.	7.9	10.4	8.0	2.6	10.4
60	−0.44	−1.08	−8.75	−65.6	n.a.	n.a.	7.4	11.7	10.0	3.9	15.7
72	−0.04	−1.25	−9.46	−67.0	n.a.	n.a.	7.4	13.5	10.7	3.7	14.7
84	−0.34	−1.50	−9.77	−69.0	9.6	9.4	8.9	7.6	4.9	0.9	3.8
89	−0.07	−1.07	−9.51	−69.5	10.9	11.7	7.2	12.3	10.9	4.5	18.0
100	−0.19	−1.48	n.a.	n.a.	n.a.	n.a.	8.5	7.6	4.7	0.7	3.0
121	−0.02	−1.17	−9.39	−68.3	9.3	9.2	8.3	10.4	7.4	2.0	8.0
126	0.04	−1.04	−9.15	−69.5	11.0	11.3	6.9	15.0	12.8	5.0	20.0
134	−0.43	−1.13	−9.58	−70.4	11.0	11.2	6.6	16.1	12.6	4.2	16.9
138	0.07	−1.26	−9.94	−71.6	11.1	10.3	7.2	13.6	9.7	2.6	10.5
139	0.10	−1.38	−9.97	−73.1	n.a.	n.a.	7.1	11.9	8.9	2.7	10.8
145	−0.10	−1.16	−9.52	−69.8	10.3	9.6	7.1	14.7	11.3	3.7	14.6
149	0.10	−1.17	−9.69	−69.0	n.a.	n.a.	7.1	15.4	12.1	4.1	16.4
151	−0.04	−0.95	−9.32	−68.0	10.1	10.6	7.0	17.4	13.7	4.7	18.6
152	−0.16	−0.93	−9.20	−67.5	10.2	10.6	7.5	14.8	12.4	4.7	18.8
154	−0.15	−1.13	−9.30	−67.4	n.a.	n.a.	8.6	16.4	11.1	2.6	10.3
165	−0.09	−1.42	−9.90	−72.8	n.a.	n.a.	7.7	9.8	6.1	1.0	4.0
179	−0.08	−1.03	−9.26	−68.3	11.1	10.5	8.0	10.9	7.6	1.9	7.7
181	−0.18	−1.13	−9.08	−69.3	n.a.	n.a.	8.7	10.6	7.6	2.1	8.4
286	−0.18	−1.11	−9.17	−68.8	n.a.	n.a.	8.5	12.9	9.1	2.4	9.6
372	0.13	−1.09	−9.09	−64.6	n.a.	n.a.	8.9	10.2	7.2	1.9	7.6
384	0.18	−1.36	n.a.	n.a.	n.a.	n.a.	8.6	8.1	5.7	1.5	6.0
442	−0.19	−1.46	−9.74	−72.0	n.a.	n.a.	8.4	9.8	5.5	0.4	1.6
453	−0.31	−1.43	−9.62	−70.3	n.a.	n.a.	8.6	9.1	5.8	1.1	4.3
478	−0.28	−1.09	n.a.	n.a.	n.a.	n.a.	7.8	9.1	6.5	1.8	7.1

n.a.: not analysed

were prepared in an identical way and followed the same analytical procedures. This identical treatment includes the use of the same background matrix as well as the same water isotopic composition for the standards and samples. The overall accuracy of the method is estimated as the reduced standard deviation of the residuals from the linear regression between the measured reference materials ($n = 16$) and their expected values. The $\delta^{15}N_{NO_3}$, $\delta^{18}O_{NO_3}$, and $\Delta^{17}O_{NO_3}$ values (^{17}O excess) of dissolved NO_3^- are given with respect to the atmospheric N_2 (AIR) and VSMOW standards, and were measured with uncertainties of ±0.5 ‰, ±2 ‰, and ±0.5 ‰, respectively.

4 Results and discussion

4.1 Ion content and mixing approach

The analysed compositions of the sampled groundwater from the Hasouna area are summarised in Table 1. The investigated Hasouna groundwater displays near-neutral pH values (pH = 7.0 ± 0.5) at temperatures between 27 and 35 °C. The concentration of dissolved oxygen is 5.5 ± 0.8 mg L^{-1} ($n = 9$). Dissolved cations and anions generally occur in the quantitative sequences of $Na^+ > Ca^{2+} > Mg^{2+} > K^+ > Sr^{2+}$ and $Cl^- > HCO_3^- > SO_4^{2-} > NO_3^-$, respectively (Table 1). The average deviation from electrical neutrality for the aqueous solutions is 3.6 meq%, with a maximum of about 5 meq %. Values less than 5 meq % indicate the good quality of ion analysis by considering the individual analytical precisions (see Sect. 3.1; Appelo and Postma, 2007). Except for NO_3^-, the chemical composition of the groundwater is within the limits for drinking water. In ≈ 85 % of the analysed Hasouna groundwater, the maximum contaminant level (MCL) of the World Health Organization (WHO, 2004) for NO_3^- in drinking water of 0.71 mM is exceeded (Table 1).

All analysed groundwater is undersaturated with respect to gypsum ($SI_{gypsum} \leq -0.93$). However, approximately 20 % of the groundwater (6 of 28 samples) is slightly supersaturated with respect to calcite ($-0.50 \leq SI_{calcite} \leq 0.18$; Table 1). If the analysed Ca^{2+} concentration is reduced by the proportion gained from $CaCO_3$ dissolution by considering the dissolution of Mg^{2+} carbonates like dolomite ($[Ca^{2+}] + [Mg^{2+}] - 0.5[HCO_3^-]$), a Ca^{2+} (reduced) to SO_4^{2-} ratio of 1 is obtained (Fig. 2). This relationship typically results from the uptake of gaseous CO_2 (e.g. in soil horizons) and the subsequent dissolution of limestone and/or dolostone (e.g. calcite and/or dolomite; Dietzel et al., 1997). Dissolution of calcite and dolomite during the evolution of the groundwater seems reasonable, as both minerals have been documented in rock core samples from Hasouna well fields (Sahli, 2006). The congruent dissolution of $CaSO_4$, like gypsum, causes the Ca^{2+} (reduced) to SO_4^{2-} ratio of 1 (Fig. 2).

The dissolved ions cover a broad concentration range, but the individual ion concentrations are well correlated. For instance, the correlation of Na^+ and Cl^- concentrations is shown in Fig. 3a. As groundwater samples #165 and #152 bracket the full observed range, their chemical composition is used for a binary mixing approach according to the expression

$$[i]_{groundwater} = x_{\#152} \cdot [i]_{\#152} + (1 - x_{\#152}) \cdot [i]_{\#165}, \quad (3)$$

where $x_{\#165} + x_{\#152} = 1$ (refer to the solid green line in Fig. 3a). In this expression [i] denotes the concentration of the dissolved ion (i is Na^+ or Cl^-) of the respective solution. The terms $x_{\#165}$ and $x_{\#152}$ are the volume fractions of groundwater samples #165 and #152, which yield the ion concentration range of the Hasouna groundwater. Analogous relationships are found for all dissolved ions (e.g. Ca^{2+} vs. NO_3^- in Fig. 3b). If seawater is assumed for a mixing end-member solution, the mixing approach of Eq. (3) fails, as in most cases the ion ratios of the groundwater are inconsistent with seawater. This is shown by the Ca^{2+} (reduced) to SO_4^{2-} ratio of the Hasouna groundwater of about 1 (Fig. 2), which differs significantly compared to that of seawater (≈ 60; assuming ancient seawater composition close to modern conditions; Drever, 2002). Additionally, an evaporation trend for #165 to reach the composition of #152 is not consistent with the measured data (dotted arrows in Fig. 3a and b). This is even valid if a decrease in Ca^{2+} concentration through calcite precipitation ($SI_{calcite} = 0$) is considered, which may be induced by evaporation (solid arrow in Fig. 3b). Thus, the solution chemistry of the Hasouna groundwater can be best explained by mixing of the two end-member solutions #165 and #152.

As an exception, the concentration of silicic acid is nearly constant in all groundwater samples ($[Si(OH)_4] = 0.22 \pm 0.02$ mM; $n = 28$) and reflects the solubility of quartz at the

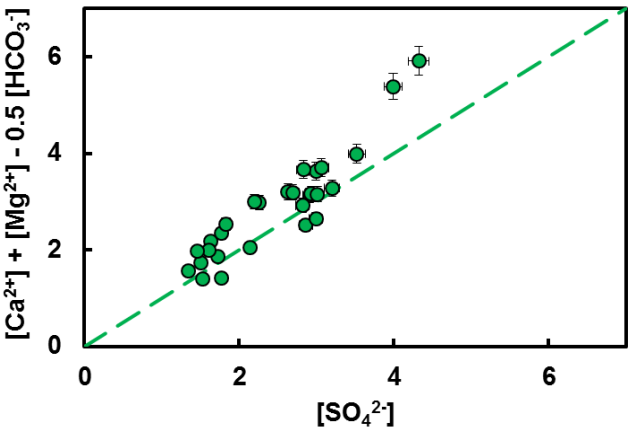

Figure 2. Ca^{2+} concentration reduced by the proportion gained from $CaCO_3$ dissolution by considering dolostone dissolution ($[Ca^{2+}] + [Mg^{2+}] - 0.5\ [HCO_3^-]$, mM) vs. the concentration of dissolved SO_4^{2-}, $[SO_4^{2-}]$ (mM). The linear relationship with a slope of 1 fits the composition of the Hasouna groundwaters quite well and reflects the dissolution of $CaSO_4$ minerals like gypsum.

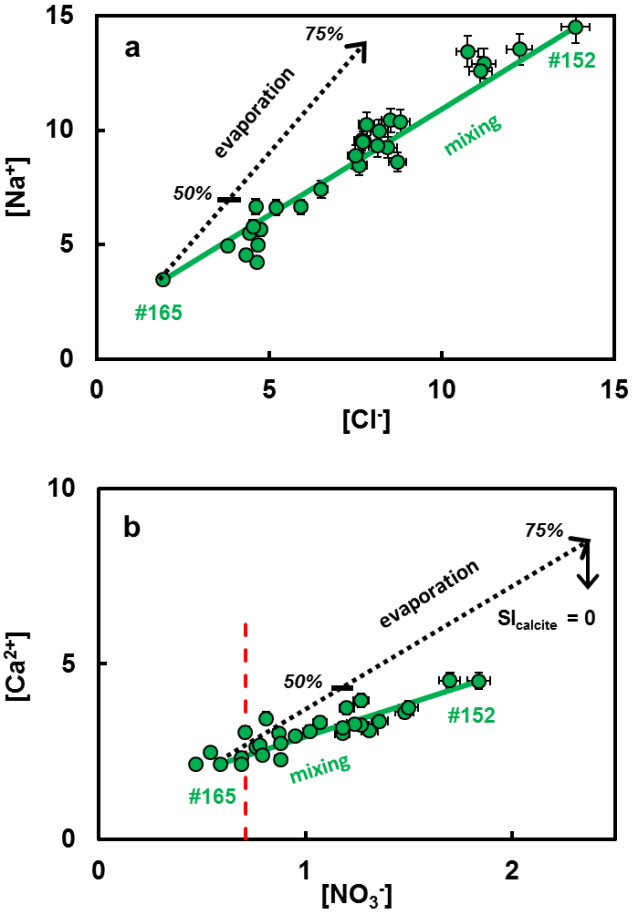

Figure 3. Chemical composition of groundwater from Hasouna, Libya. **(a)** Na^+ vs. Cl^- concentration. **(b)** Ca^{2+} vs. NO_3^- concentration. Values are given in mM. Solid green lines: mixing between end-member solutions #165 and #152 with the lowest and highest ion concentrations, respectively. Dotted arrows: chemical trend for evaporation of solution #165, where 50 and 75 % denote ion concentrations at the respective loss of H_2O by evaporation. Solid arrow: Decrease in Ca^{2+} concentration by considering calcite precipitation to reach $SI_{calcite} = 0$. Dashed red line: MCL for NO_3^- in drinking water according to the WHO (WHO, 2004).

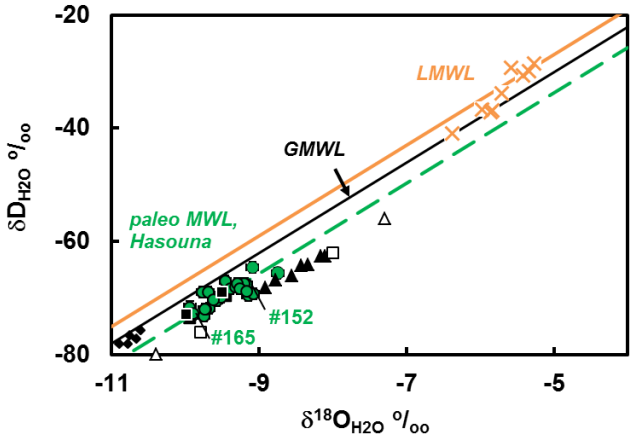

Figure 4. Stable hydrogen and oxygen isotope composition of groundwater from North Africa. Paleo-groundwater displays lower stable isotope values and an elevated d excess compared to modern precipitation, which indicates recharge under cooler and more humid climate conditions vs. modern climate conditions. The analytic inaccuracies for δD_{H_2O} (±0.8 ‰) and $\delta^{18}O_{H_2O}$ (±0.05 ‰) lay within the size of the symbols. Isotope composition of modern eastern Mediterranean seawater is outside the displayed range, comprising $\delta^{18}O$ values from 0.3 to 2.5 ‰ and δD values ≈ 0 ‰ (Gat, 2010). ●: Hasouna, Libya (this study); ■: Hasouna, Libya, isotope range (Milne-Home and Sahli, 2007); □: Murzuq Basin, Libya, isotopic range (Sonntag et al., 1978); △: Arab Jamahiriya, Libya (Srdoè et al., 1980); ▲: Southern Tunisia (Abid et al., 2012); ♦: Wadi Ash Shati Valley, Libya (Salem et al., 1980). X: Groundwater recharged by modern precipitation close to Tripoli (own data). GMWL: Global Meteoric Water Line ($\delta D_{H_2O} = 8\ \delta^{18}O_{H_2O} + 10$; Craig, 1961). LMWL: Local Meteoric Water Line for Sfax metereological station, southern Tunisia (yellow line: $\delta D_{H_2O} = 8\ \delta^{18}O_{H_2O} + 13$; Abid et al., 2012). Paleo MWL: Paleo Meteoric Water Line estimated from isotopic data of the present study by the least squares method (dashed green line: Eq. 4).

average temperature of the Hasouna groundwater ($K_{quartz} = [Si(OH)_4] = 0.22$ mM at 31 °C; Rimstidt, 1997). Thus, the concentrations of silicic acid in the ancient Hasouna groundwater from the Nubian Sandstone Aquifer are clearly controlled by quartz–water interaction considering thermodynamic equilibrium, which is typically found for ancient groundwater in quartz-dominated aquifers (Rimstidt, 1997, and references therein).

4.2 Stable isotopes of water and climate record

The δD_{H_2O} and $\delta^{18}O_{H_2O}$ values of the analysed Saharan groundwater range from −73.2 to −64.6 ‰ and from −9.97 to −8.75 ‰, respectively (Table 1). The isotope values fall below the modern Global Meteoric Water Line (GMWL) and Local Meteoric Water Line (LMWL is given for Sfax, southern Tunisia; see Fig. 4). Our isotope data are very close to former results reported for paleo-groundwater from Hasouna, Murzuq Basin, Wadi Ash Shati Valley, Arab Jamahiriya in Libya and paleo-groundwater from southern Tunisia (Abid et al., 2012; Milne-Home and Sahli, 2007; Salem et al., 1980; Sonntag et al., 1978; Srdoč et al., 1980). From the isotope composition of our Hasouna groundwater the local Paleo Meteoric Water Line

$$\delta D_{H_2O} = 8.0\ \delta^{18}O_{H_2O} + 6.3, \quad R^2 = 0.82 \qquad (4)$$

is estimated (see Fig. 4). The lower deuterium excess (d excess = 6.3 = $\delta D - 8.0\ \delta^{18}O$) for the paleo-groundwater compared to that of modern precipitation (12 ± 2 ‰) is caused by decreasing moisture deficit (increase in relative humidity) of the air above sea water during evaporation (Sonntag et al., 1978). As air moisture deficit is positively correlated with temperature, a lower paleo-temperature and

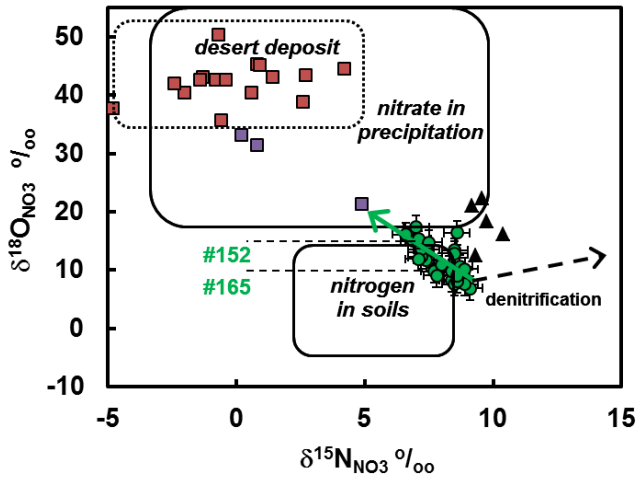

Figure 5. $\delta^{18}O_{NO_3}$ vs. $\delta^{15}N_{NO_3}$ values in NO_3^- (adapted from Kendall, 1998). $\delta^{18}O_{NO_3}$ and $\delta^{15}N_{NO_3}$ values are referred to the VSMOW and AIR standards, respectively. ●: Hasouna groundwater (this study), where the solid green arrow displays the regression line ($\delta^{18}O_{NO_3} = -2.79\ \delta^{15}N_{NO_3} + 33.8$) and an increase in NO_3^- concentration; ▲: Hasouna groundwater (Milne-Home and Sahli, 2007); ■ and ■: NO_3^--rich deposit of the Atacama (Chile) and Mojave deserts (California), respectively (Böhlke et al., 1997).

higher paleo-humidity are suggested from the lower d excess (Kendall and Doctor, 2004).

In accordance with the overall shift of Saharan paleo-groundwater to low δD_{H_2O} and $\delta^{18}O_{H_2O}$ values compared to apparent local precipitation (in Sfax and Tripoli, Fig. 4), it is postulated that the Hasouna groundwater was recharged under paleoclimatic conditions, which were cooler and much more humid compared to the modern situation (Clark and Fritz, 1997; Edmunds, 2006). In accordance with the above-mentioned mixing approach, an evaporation effect for Hasouna paleo-groundwater (e.g. subsequent to precipitation or during infiltration) can be ruled out, as the slope of the regression line for the isotope data is similar to the MWLs (Craig, 1961; Kendall and Doctor, 2004).

4.3 Stable isotopes of nitrate, origin and potential overprints

The $\delta^{18}O_{NO_3}$ and $\delta^{15}N_{NO_3}$ values of the dissolved NO_3^- for the Hasouna groundwater range from 6.9 to 17.4 ‰ and from 6.6 to 9.1 ‰, respectively, and are shown in Fig. 5 in relation to the isotope ranges of different sources for NO_3^- (see Kendall, 1998 and Böhlke et al., 1997). Our measured $\delta^{15}N_{NO_3}$ and $\delta^{18}O_{NO_3}$ values are almost within the range of a microbial origin for NO_3^- (e.g. obtained by nitrification in soils), where $^{18}O/^{16}O$ is incorporated from the reacting H_2O and O_2, and the $\delta^{15}N_{NO_3}$ value is derived from organic matter (Fig. 5).

In modern groundwater the isotope composition of NO_3^- might be modified within pyrite-bearing aquifers by microbial NO_3^- reduction via oxidation of iron sulphides according to the idealised overall reaction

$$5\ FeS_2 + 14\ NO_3^- + 4\ H^+ \rightarrow 5\ Fe^{2+} + 7\ N_{2(g)} + 10\ SO_4^{2-} + 2\ H_2O \quad (5)$$

(Böttcher et al., 1990; Zhang et al., 2010, 2012; Saccon et al., 2013). This overprint can be followed by a characteristic superimposition of the sulfur and oxygen isotope composition of dissolved SO_4^{2-} (e.g. Zhang et al., 2011, 2012). The measured narrow range of $\delta^{34}S_{SO_4}$ and $\delta^{18}O_{SO_4}$ values in Hasouna groundwater of $+10.5 \pm 0.7$ ‰ vs. VCDT and $+10.4 \pm 0.8$ ‰ vs. VSMOW ($n = 10$; see Table 1), respectively, is surprising, considering the observed wide range in SO_4^{2-} concentrations (1.3 to 4.3 mM, see Fig. 6). In addition, no significant correlation of the above isotope data with the NO_3^- concentrations exists. This behaviour indicates that the source of dissolved SO_4^{2-} was not coupled to NO_3^- reduction. Thus pyrite oxidation-driven NO_3^- reduction is considered to be insignificant. In addition, the heavy sulfur isotope values exclude significant contributions, at least from biogenic pyrite oxidation. If isotopically light sulfur would have been modified by later microbial SO_4^{2-} reduction under essentially closed system conditions (e.g. Hartmann and Nielsen, 2012) to reach heavy residual SO_4^{2-} values, one would expect an equilibration of the oxygen isotope signature of SO_4^{2-} with the surrounding bulk water (Fritz et al., 1989). Using the fractionation factors derived by Fritz et al. (1989) much heavier oxygen isotope values for water are expected. The isotope data of the dissolved SO_4^{2-} are close to values reported for Permian evaporites (Böttcher, 1999; Mittermayr et al., 2012; Nielson, 1979; $\delta^{34}S_{SO_4} = +11 \pm 1$ ‰), but differ significantly from the isotope values of modern Mediterranean seawater $\delta^{34}S_{SO_4} = +21$ ‰; Böttcher et al., 1998; Fig. 6). Unfortunately, details regarding the hydrogeological conditions of the groundwater remain unknown, in particular with respect to the regional occurrence and distribution of $CaSO_4$ horizons. However, our hydrogeochemical findings and isotope values support the dissolution of gypsum during subterranean groundwater evolution, as shown by the relationship in Fig. 2. Moreover, the correlation for the concentrations of dissolved Sr^{2+} vs. Ca^{2+} of Hasouna groundwater ($[Sr^{2+}] = 0.0058 \cdot [Ca^{2+}]$, $R^2 = 0.83$; see values in Table 1) is typically found where evaporite gypsum deposits are dissolved (e.g. Dietzel and Kirchhoff, 2003). Thus, from the solution chemistry of the groundwater as well as from the known occurrence of evaporites on the Saharan platform (Turner and Sherif, 2007), and occasionally documented gypsum in core samples from Hasouna well fields (Sahli, 2006), we reasonably assume salt dissolution to be the dominant source of the dissolved SO_4^{2-}. This conclusion is also supported by the above-mentioned narrow range of stable isotope data with respect to SO_4^{2-}, with no correlation of isotope data and SO_4^{2-} concentrations (Fig. 6).

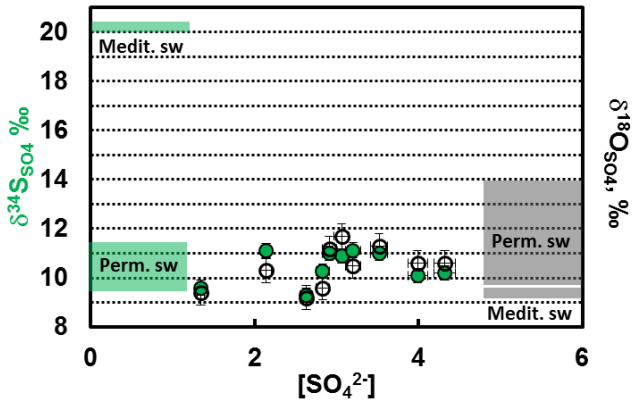

Figure 6. The isotope composition as a function of the concentration of dissolved SO_4^{2-}. Green and open circles denote $\delta^{34}S_{SO_4}$ (VCDT) and $\delta^{18}O_{SO_4}$ (VSMOW) values, respectively. The presented $\delta^{34}S_{SO_4}$ and $\delta^{18}O_{SO_4}$ ranges of dissolved SO_4^{2-} of modern Mediterranean seawater (Medit. sw) and Permian SO_4^{2-} (Perm. sw) are from Böttcher et al. (1998), Böttcher (1999), Faure and Mensing (2005), Mittermayr et al. (2012), and Nielson (1979).

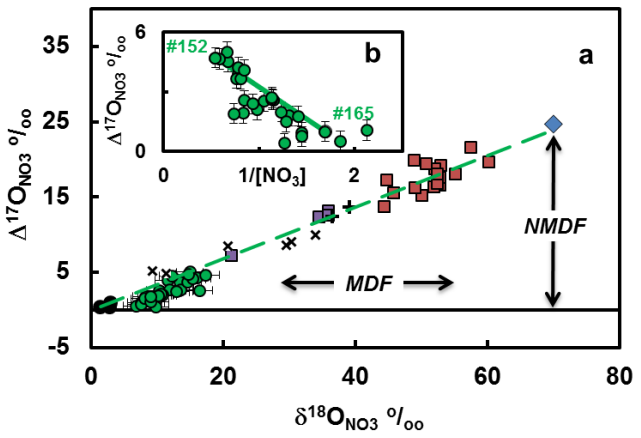

Figure 7. (a) ^{17}O excess ($\Delta^{17}O_{NO_3}$) vs. $\delta^{18}O_{NO_3}$ value of Hasouna groundwaters. **(b)** Mixing approach for the #165 and #152 end-member solutions, where the ^{17}O excess of dissolved NO_3^- and the reciprocal NO_3^- concentration (mM) can be followed by a linear relationship. Isotope values are related to the VSMOW standard. ●: Hasouna groundwater, Libya (this study). ■ and ■: NO_3^--rich deposit of the Atacama (Chile) and Mojave (California) deserts, respectively (Michalski et al., 2004a). •: Groundwater from the Mojave Desert (Michalski et al., 2004a). **x**: Stream water from San Gorgonio and Devil Canyon at storm flow events (California; Michalski et al., 2004b). +: NO_3^--rich deposit of Kumutag (China; Li et al., 2010). ♦: Atmospheric photochemical NO_3^- (Michalski et al., 2004a). Solid horizontal line: terrestrial isotope fractionation line considering MDF. Dashed green line: regression line for all given data ($\Delta^{17}O_{NO_3} = 0.342\,\delta^{18}O_{NO_3}$; $R^2 = 0.978$).

A pronounced trend toward higher $\delta^{18}O_{NO_3}$ and lower $\delta^{15}N_{NO_3}$ values is obvious for elevated NO_3^- concentrations (solid green arrow in Fig. 5). This trend cannot result from denitrification (dashed arrow; Böttcher et al., 1990; Kendall,1998; Granger et al., 2010), but might be explained by an impact of NO_3^- from atmospheric deposition (e.g. Böhlke et al., 1997).

The origin of NO_3^- can be constrained by considering the ^{17}O isotope, and evaluating both the $\delta^{17}O_{NO_3}$ and $\delta^{18}O_{NO_3}$ values (see Eq. (1)). All Hasouna paleo-groundwater measured here exhibits a positive ^{17}O excess up to $\Delta^{17}O_{NO_3} \approx 5$ ‰, which is attributed to NMDF during the conversion of atmospheric NO_x and O_3 to $NO_{3\,(atm)}^-$ (Table 1; Kendall and Doctor, 2004; Michalski et al., 2004a; Thiemens, 2001). In Fig. 7a, the ^{17}O excess vs. the traditional $\delta^{18}O_{NO_3}$ value is displayed. A potential secondary (de)nitrification or reduction impact can be followed by a shift parallel to the terrestrial fractionation trend (horizontal arrows indicate the MDF effect). For the given isotope data of NO_3^- in Fig. 7a, an overall relationship with a slope of 0.342 is obtained from least squares regression, which fits well with the $\Delta^{17}O_{NO_3}$ end member, the atmospheric photochemical NO_3^- (Michalski et al., 2004a; see Fig. 7a). The deviation from the overall correlation of isotope data, which is given by the green dashed line in Fig. 7a, can be explained by MDF effects. The isotope data of Hasouna groundwater plot slightly below the dashed line. This behaviour may be caused by minor variability of the isotopic composition of atmospheric photochemical NO_3^- and/or by a slight impact on secondary MDF effects, e.g. induced by denitrification. For the present case the overall nonrelevance of denitrification is shown in Fig. 5.

The formation of $NO_{3,atm}^-$ is linked to the most important oxidant in the atmosphere: O_3. The respective $\Delta^{17}O$ of atmospheric NO_3^-, gained from the conversion of atmospheric NO_x and O_3, can be followed by three major reaction pathways involving NO_2, O_3, OH^- and H_2O (Gao and Marcus, 2001; Savarino, 2000; Michalski et al., 2003). The proportion of $NO_{3,atm}^-$ for the former reaction paths and corresponding precipitation rates can be obtained from global climate models, which finally results in $\Delta^{17}O_{NO_{3,atm}}$ of about +25 ‰, a value well corroborated by atmospheric observations (Michalski et al., 2003; Morin et al., 2008; Alexander et al., 2009). In contrast, microbially induced nitrification in soils results in $\Delta^{17}O_{NO_{3,soil}} = 0$ ‰. The individual ^{17}O excess of dissolved NO_3^- of the analysed Saharan groundwater, $\Delta^{17}O_{NO_3}$, can be used to calculate the fraction of atmospheric NO_3^- vs. the total NO_3^- concentration according to the expression $\Delta^{17}O_{NO_3}$.

$$x[NO_3^-]_{atm} = \frac{\Delta^{17}O_{NO_3}}{\Delta^{17}O_{NO_{3,atm}}} \cdot 100\,(\%) \qquad (6)$$

Considering the measured $\Delta^{17}O_{NO_3}$ values of the groundwater from 0.4 to 5 ‰ in Table 1 and $\Delta^{17}O_{NO_{3,atm}} \approx +25$ ‰, individual proportions from 1.6 up to 20.0 % for atmospheric

origin with respect to the total dissolved NO_3^- are obtained. The remaining NO_3^- proportion is referred to recycled NO_3^- in soil horizons, where oxygen isotopes in NO_3^- are incorporated via microbially induced nitrification from the reacting H_2O and O_2. Interestingly, $x[NO_3^-]_{atm} \approx 20\,\%$ is consistent with the proportion of non-recycled atmospheric NO_3^- vs. total NO_3^- estimated from $\delta^{18}O_{NO_3}$ data of unsaturated zone moisture in the arid Badain Jaran Desert (China; Gates et al., 2008). The $\Delta^{17}O_{NO_3}$ values of dissolved NO_3^- in the Hasouna Aquifer thus clearly reveal that NO_3^- is a mixture between NO_3^- transferred from the atmosphere and NO_3^- gained from nitrification.

5 Implications for paleo-climate conditions during recharge

In analogy to the ion concentrations, a binary mixing approach that considers end-member solutions #165 and #152 is consistent with the ^{17}O excess in Hasouna paleo-groundwater. This mixing approach is displayed by a linear correlation of $\Delta^{17}O_{NO_3}$ values vs. $1/[NO_3^-]$ in Fig. 7b, where elevated $NO_{3,atm}^-$ proportions (higher ^{17}O excess) are obtained at high total NO_3^- concentrations (e.g. groundwater #152). Such elevated $NO_{3,atm}^-$ proportions can be explained by an impact of flood events as shown by Michalski et al. (2004b) from monitored values during storm events in the Devil Canyon watershed (southern California, USA). $\Delta^{17}O_{NO_3}$ maximum values are caused by a wash-out of dry deposition of atmospheric NO_3^-, which was accumulated through long-term arid conditions to which plant and soil surfaces had been exposed. Periodic infiltration events enhanced the leaching of accumulated NO_3^- from plant and soil surfaces and also from below the near-surface and rooting zone. Accordingly, the NO_3^--enriched solutions migrated downward through the vadose zone to the water table and correspondingly high NO_3^- concentrations occur in the recharging groundwater (see also Edmunds and Gaye, 1997, Tyler et al., 1997, Hartsough et al., 2001, Walvoord et al., 2003 and Chiwa et al., 2010).

For the present case, it is proposed that dry periods have alternated with periodic infiltration events in wetter climates, where infiltration of solutions occurred leaving the ^{17}O excess of NO_3^- preserved. These environmental conditions during recharge coincide well with results from pollen analyses in the Sahara Desert (Libya), where past climate oscillations between wet and dry periods are documented at about 8–10 ka BP (Mercuri, 2008). Preserved $\Delta^{17}O_{NO_3} > 0\,‰$ clearly indicates that $NO_{3,atm}^-$ underwent limited biological processing, as the time for infiltration through soil horizons was limited (Michalski et al., 2004b). Limited NO_3^-–biotic interaction periods are confirmed by the uniform sulfur and oxygen isotope composition of SO_4^{2-} and in particular by $\delta^{18}O_{NO_3}$ values, which change in the direction to atmospheric NO_3^- at elevated NO_3^- concentrations. The latter relationship is opposite to what would be expected to occur during denitrification (Fig. 5).

The local distribution of $x[NO_3^-]_{atm}$ (Eq. 6) is analogous to that of the NO_3^- content shown in Fig. 1, as $\Delta^{17}O_{NO_3}$ is negatively correlated to $1/[NO_3^-]$ (see Fig. 7b). Spatial variability in $x[NO_3^-]_{atm}$ and $[NO_3^-]$ is attributed to paleoclimatic conditions during recharge and to an associated paleo-biosphere response. A relative increase in $x[NO_3^-]_{atm}$ can be caused by (i) longer lasting dry periods with subsequent precipitation events and/or (ii) a local surface covered by less fertile soils. High $\Delta^{17}O_{NO_3}$ values of Hasouna groundwater reflect soils more barren in the dry periods, while low $\Delta^{17}O_{NO_3}$ values correspond to more fertile soils. Combining the climate record from the isotope composition of the water with the $\Delta^{17}O_{NO_3}$ data, elevated $x[NO_3^-]_{atm}$ values are correlated with less negative δD_{H_2O} and $\delta^{18}O_{H_2O}$ values (see groundwater samples #152 vs. #165 in Figs. 4 and 7b). This relationship traces longer lasting dry periods and more barren soils for these dry periods under relatively warmer climate conditions.

6 Conclusions

In the present study we used an integrated hydrogeochemical and isotope approach to trace the origin of NO_3^- and to reconstruct the paleoclimatic conditions during recharge of Saharan groundwater in the area of Hasouna, Libya. We applied the outstanding feature of $\Delta^{17}O_{NO_3}$ values to trace atmospheric NO_3^-, as the ^{17}O excess of dissolved NO_3^- is not affected by terrestrial fractionation processes (MDF) (Kendall and Doctor, 2004). Our ^{17}O-excess data clearly show that in the present Saharan groundwater up to 20 mol % of the dissolved NO_3^- originates from the atmosphere, with the remaining NO_3^- being leached from the soils (Table 1). To our knowledge, this is the first study where ^{17}O excess of NO_3^- is measured in paleo-groundwater, verifying that $\Delta^{17}O_{NO_3}$ values survived up to thousands of years and can still be used to estimate the $NO_{3,atm}^-$ proportion of total dissolved NO_3^- during ancient recharge. Aerobic conditions documented by the presence of dissolved O_2 and the isotope composition of dissolved SO_4^{2-} within the Saharan aquifer have allowed dissolved NO_3^- from paleo-recharge to persist until the present. This nitrogen trap has formed a still underestimated N reservoir for N cycling and balancing (see also Gates et al., 2008). The NO_3^- content within the aquifer is predetermined by paleo-recharge conditions. Thus, for the management of water supply by using Saharan groundwater from Hasouna well fields, elevated NO_3^- concentrations have to be considered as a long-lasting challenge.

The assumption of groundwater mixing within the aquifer seems to be reasonable, considering that paleo-groundwater with a huge variability in salinity is regionally documented.

For instance, for the Zimam aquifer with enhanced salinities and elevated NO_3^- concentrations up to 1.1 mM (El-Baruni et al., 1985; located close to #152), significant leakage into the underlying Cambro–Ordovician sandstone aquifer through fractures in limestone and dolostone is postulated (Binsariti and Saeed, 2000). To understand the groundwater evolution in more detail, a sophisticated modelling approach using more refined age models and all respective hydrogeochemical parameters must be considered.

An evaporation trend is reflected by neither solution chemistry nor the δD_{H_2O}–$\delta^{18}O_{H_2O}$ relationship. Low d excess as well as low δD_{H_2O} and $\delta^{18}O_{H_2O}$ values indicate that the groundwater of the Hasouna basin was recharged under cooler and more humid climates compared to the current conditions along the coastal areas of Libya. The negative correlation between $\Delta^{17}O_{NO_3}$ values and reciprocal NO_3^- concentrations traces longer lasting dry periods, and more barren soils corresponding to warmer climate conditions. Past alternating arid periods and infiltration events are suggested, which lead to the observed isotope values. The accumulated $NO_{3,atm}^-$ is washed out from plant and soil surfaces as well as below the near-surface and rooting zone downward through the vadose zone to the water table. A rapid infiltration through the subsurface without significant evaporation of water had recharged the Saharan paleo-groundwater of Hasouna.

Acknowledgements. We wish to thank Al Mahdi Megrbi of the General Water Authority (Tripoli, Libya) and in particular Omar Salem for the permission to collect groundwater samples from the Hasouna well field area and for administrative arrangements. Support from the Authority of the Great Man-made River Project in Tripoli and from Christian Schmid (Leoben, Austria) with respect to logistics and field work is greatly appreciated. Thomas Max (MPI Bremen) is thanked for his technical support. This work was financially supported by the Graz University of Technology (Austria) scientific grant programme. Chemical analyses were carried out at the NAWI Graz Central Lab for Water, Minerals and Rocks. The Institut National des Sciences de l'Univers (INSU) is acknowledged for funding the isotope analysis of NO_3^- performed in the laboratory of Joel Savarino and Samuel Morin through the LEFE/CHAT programme. LGGE and CNRM-GAME/CEN are part of LabEx OSUG@2020 (ANR10 LABX56). The proofreading of Scott Kieffer is greatly appreciated. The authors thank Scott Tyler and two anonymous reviewers for their constructive comments on the manuscript.

Edited by: D. Obrist

References

Abdelrhem, I. M., Raschid, K., and Ismail, A.: Integrated groundwater management for great man-made river project in Libya, Eur. J. Sci. Res., 22 562–569, 2008.

Abid, K., Dulinski, M., Ammar, F. H., Rozanski, K., and Zouari, K.: Deciphering interaction of regional aquifers in southern Tunisia using hydrochemistry and isotopic tools, Appl. Geochem., 27, 44–55, 2012.

Alexander, B., Hastings, M. G., Allman, D. J., Dachs, J., Thornton, J. A., and Kunasek, S. A.: Quantifying atmospheric nitrate formation pathways based on a global model of the oxygen isotopic composition ($\Delta^{17}O$) of atmospheric nitrate, Atmos. Chem. Phys., 9, 5043–5056, doi:10.5194/acp-9-5043-2009, 2009.

Amberger, A. and Schmidt, H. L.: Natürliche Isotopengehalte von Nitrat als Indikatoren für dessen Herkunft, Geochim. Cosmochim. Ac., 51, 2699–2705, 1987.

Appelo, C. A. J. and Postma, D.: Geochemistry, groundwater and pollution, Balkema, Rotterdam 649 pp., 2007.

Binsariti, A. and Saeed, F. S.: Groundwater salinity variations in the cambro-ordovician aquifer of eastern jabal al hasawnah, the great man-made river project, Libya in: Geological Exploration in Murzuq Basin, edited by: Sola, M. A. and Worsley, D., 1–16, 2000.

Blackwell, B. A. B., Skinner, A. R., Mashriqi, F., Deely, A. E., Long, R. A., Gong, J. J. J., Kleindienst, M. R., and Smith, J. R.: Challenges in constraining pluvial events and hominin activity: examples of ESR dating molluscs from the western desert, Egypt, Quat. Geochronol., 10, 430–435, 2012.

Boehlke, J. K., Ericksen, G. E., and Revesz, K.: Stable isotope evidence for an atmospheric origin of desert nitrate deposits in northern Chile and southern California, USA, Chem. Geol., 136, 135–152, 1997.

Böttcher, J., Strebel, O., Voerkelius, S., Schmidt, H. L.: Using stable isotope fractionation of nitrate – nitrogen and nitrate – oxygen for evaluation of microbial denitrification in a sandy aquifer, J. Hydrol., 114, 413–424, 1990.

Böttcher, M. E., Thamdrup, B., and Vennemann, T. W.: Oxygen and sulfur isotope fractionation during anaerobic bacterial disproportionation of elemental sulfur, Geochim. Cosmochim. Acta, 65, 1601-1609, 2001.

Böttcher, M. E., Brumsack, H.-J., and Lange, G. J.: Sulfate reduction and related stable isotope (^{34}S, ^{18}O) variations in interstitial waters from the eastern Mediterranean, in: Proceedings of Ocean Drilling Programm, Scientific Results, 160, edited by: Robertson, A. H. F., Emeis, K., Richter, C., and Camerlenghi, A., 365–373, 1998.

Carrara, C., Cremaschi, M., and Quinif, Y.: The travertine deposits in the Tadrart Acacus (Libyan Sahara), nature and age, in: Wadi Teshuinat – Palaeoenvironment and Prehistory in South-Western Fezzan (Libyan Sahara), edited by: Cremaschi, M. and Di Lernia, S., C. N. R. Quaderni di Geodinamica Alpina e Quaternaria, 7, 59–66, 1998.

Casciotti, K. L., Sigman, D. M., Hastings, M. G., Böhlke, J. K., and Hilkert, A.: Measurement of the oxygen isotopic composition of nitrate in seawater and freshwater using the denitrifier method, Anal. Chem., 74, 4905–4912, 2002.

Chiwa, M., Ide, J., Maruno, R., Higashi, N., and Otsuki, K.: Effects of storm flow samplings on the evaluation of inorganic nitrogen and sulfate budgets in a small forested watershed, Hydrol. Process., 24, 631–640, 2010.

Clark, I. D. and Fritz, P.: Environmental Isotopes in Hydrology, CRC Press, 352 pp., 1997.

Craig, H.: Isotopic variations in meteoric waters, Science, 133, 1702–1703, 1961.

Darrouzet-Nardi, A., Erbland, J., Bowman, W., Savarino, J. and Williams, M.: Landscape-level nitrogen import and export in an ecosystem with complex terrain, Colorado Front Range, Biogeochemistry, 109, 271–285, doi:10.1007/s10533-011-9625-8, 2012.

Dejwakh, N. R., Meixner, T., Michalski, G., and McIntosh, J.: Using O-17 to investigate nitrate sources and sinks in a semi-arid groundwater system, Environ. Sci. Technol., 46, 745–751, 2012.

Dietzel, M. and Kirchhoff, T.: Stable isotope ratios and the evolution of acidulous solutions, Aquat. Geochem., 8, 229–254, 2003.

Dietzel, M., Kolmer, H., Pölt, P., and Simic, S.: Desert varnish and petroglyphs on sandstone – geochemical composition and climate changes from Pleistocene to Holocene (Libya), Geochemistry, 68, 31–43, 2008.

Dietzel, M., Schwecke, H., Hirschfeld, A., Röhring, M., and Böttcher, M. E.: Geochemische und $^{13}C/^{12}C$-isotopenchemische Untersuchung zur Herkunft der Kohlensäure in mineralhaltigen Wässern Nordhessens (Deutschland), Acta Hydroch. Hydrob., 25, 191–201, 1997.

Doherty, R., Kutzbach, J., Foley, J., and Pollard, D.: Fully coupled climate/dynamical vegetation model simulations over northern Africa during the mid-Holocene, Clim. Dynam., 16, 561–573, 2000.

Drever, J.: The Geochemistry of Natural Waters, Practice Hall, 3rd edn., 436 pp., 2002.

Edmunds, W. M.: Libya's Saharan groundwater: occurrence, origins and outlook, in: The Libyan Desert: Natural Resources and Cultural Heritage, edited by: Mattingly, D., McLaren, S., and Savage, E., Society of Libyan Studies Monograph, 45–64, 2006.

Edmunds, W. M. and Gaye, C. B.: Naturally high nitrate concentrations in groundwaters from the Sahel, J. Environ. Qual., 26, 1231–1239, 1997.

Edmunds, W. M., Dodo, A., Djoret, D., Gasse, F., Gaye, C. B., Goni, I. B., Travi, Y., Zouari, K., and Zuppi, G. M.: Groundwater as an archive of climatic and environmental change, in: Past Climate Variability Through Europe and Africa, Developments in Paleoenviromental Research, edited by: Battarbee, R. W., Gasse, F., and Stickly, C. E., Kluwer, Dordrecht, 279–306, 2003.

Edmunds, W. M. and Wright, E. P.: Groundwater recharge and palaeoclimate in the Sirte and Kufra basins, Libya, J. Hydrol., 40, 215–241, 1979.

El-Baruni, S. S., El-Futasi, R. H., and Maaruf, A. M.: Hydrology of Ghadamis basin, NW Libya, in: Geology of Libya, Libyan Arab Jamahiriya, Tripoli, 269–290, 1985.

Erbland, J., Vicars, W. C., Savarino, J., Morin, S., Frey, M. M., Frosini, D., Vince, E., and Martins, J. M. F.: Air-snow transfer of nitrate on the East Antarctic Plateau – Part 1: Isotopic evidence for a photolytically driven dynamic equilibrium in summer, Atmos. Chem. Phys., 13, 6403–6419, doi:10.5194/acp-13-6403-2013, 2013.

Faure, G. and Mensing, T. M.: Isotopes, Principles and Applications, Wiley and Sons Inc., 3rd edn., 897 pp., 2005.

Frey, M. M., Savarino, J., Morin, S., Erbland, J. and Martins, J. M. F.: Photolysis imprint in the nitrate stable isotope signal in snow and atmosphere of East Antarctica and implications for reactive nitrogen cycling. Atmos Chem Phys 9, 8681–8696, 2009.

Fritz, P., Basharmnal, G. M., Drimmie, R. J., Ibsen, J., and Qureshi, R. M.: Oxygen isotope exchange between sulphate and water during bacterial reduction of sulphate, Chem. Geol., 79, 99–105, 1989.

Gao, Y. Q. and Marcus, R. A.: Strange and unconventional isotope effects in ozone formation, Science, 293, 259–263, 2001.

Gat, J. G.: Isotope Hydrology, a Study of Water Cycle, Imperial College Press, 189 pp., 2010.

Gates, J. B., Böhlke, J. K., and Edmunds, W. M.: Ecohydrological factors affecting nitrate concentrations in a phreatic desert aquifer in northwestern China, Environ. Sci. Technol., 42, 3531–3537, 2008.

Granger, J., Sigman, D. M., Rohde, M. M., Maldonado, M. T., and Tortell, P. D.: N and O isotope effects during nitrate assimilation by unicellular prokaryotic and eukaryotic plankton cultures, Geochim. Cosmochim. Ac., 74, 1030–1040, 2010.

Guendouz, A., Moulla, A. S., Edmunds, W. M., Shand, P., Poole, J., Zouari, K., and Mamou, A.: Palaeoclimatic information contained in groundwaters of the Grand Erg Oriental, north Africa, in: Isotope Techniques in the Study of Environmental Change, IAEA, Vienna, 555–571, 1998.

Hartmann, M. and Nielsen, H.: $\delta^{34}S$ values in recent sea sediments and their significance using several sediment profiles from the western Baltic Sea, Isot. Environ. Healt. St., 48, 7–32, 2012.

Hartsough, P., Tyler, S. W., Sterling, J., and Walvoord, M.: A 14.6 kyr record of nitrogen flux from desert soil profiles as inferred from vadose zone pore waters, Geophys. Res. Lett., 28, 2955–2958, 2001.

Horita, J., Ueda, A., Mizukami, K., and Takatori, I.: Automatic δD and $\delta^{18}O$ analyses of multi-water samples using H_2- and CO_2-water equilibration methods with a common equilibration set-up, Appl. Radiat. Isotopes, 40, 801–805, 1989.

Kaiser, J., Hastings, M. G., Houlton, B. Z., Röckmann, T., and Sigman, D. M.: Triple oxygen isotope analysis of nitrate using the denitrifier method and thermal decomposition of N_2O, Anal. Chem., 79, 599–607, 2007.

Kendall, C.: Tracing nitrogen sources and cycling in catchments, in: Isotope Tracers in Catchment Hydrology, edited by: Kendall, C. and McDonnell, J. J., 519–576, 1998.

Kendall, C. and Doctor, D. H.: Stable isotope applications in hydrologic studies, in: Treatise on Geochemistry – Surface and Groundwater, Weathering and Soils, edited by: Drever, J. I., 319–364, 2004.

Kornexl, B. E., Gehre, M., Hofling, R., and Werner, R. A.: On-line delta O-18 measurement of organic and inorganic substances, Rapid Commun. Mass Sp., 13, 1685–1693, 1999.

Kuper, R. and Kröpalin, S.: Climate-controlled Holocene occupation in the Sahara: motor of Africa's evolution, Science, 313, 803–807, 2006.

Li, Y. H., Qin, Y., Liu, F., Hou, K. J., and Wan, D. F.: Discovery of mass independent oxygen isotopic compositions in superscale nitrate mineral deposits from Turpan-Hami basin, Xinjiang, China and its significance, Acta Geol. Sin.-Engl., 84, 1514–1519, 2010.

Lourens, L. J., Wehausen, R., and Brumsack, H.-J.: Geological constraints on tidal dissipations and dynamical ellipticity of the Earth over the past three million years, Nature, 409, 1029–1033, 2001.

Mercuri, A. M.: Human influence, plant landscape evolution and climate inferences from the archaeobotanical records of the Wadi

Teshuinat area (Libyan Sahara), J. Arid Environ., 72, 1950–1967, 2008.

Michalski, G., Scott, Z., Kabiling, M., and Thiemens, M. H.: First measurements and modeling of δ^{17}O in atmospheric nitrate, Geophys. Res. Lett., 30, 14–11, 2003.

Michalski, G., Bohlke, J. K., and Thiemens, M.: Long term atmospheric deposition as the source of nitrate and other salts in the Atacama desert, Chile: new evidence from mass-independent oxygen isotopic compositions, Geochim. Cosmochim. Ac., 68, 4023–4038, 2004a.

Michalski, G., Meixner, T., Fenn, M., Hernandez, L., Sirulnik, A., Allen, E., and Thiemens, M.: Tracing atmospheric nitrate deposition in a complex semiarid ecosystem using δ^{17}O, Environ. Sci. Technol., 38, 2175–2181, 2004b.

Michalski, G., Bockheim, J. G., Kendall, C., and Thiemens, M.: Isotopic composition of Antarctic dry valley nitrate: implications for NO(y) sources and cycling in Antarctica, Geophys. Res. Lett., 32, 4, 2005.

Milne-Home, W. A. and Sahli, N. I. M.: Application of ^{15}N isotopes to management of groundwater quality Hasouna wellfields, Great Man-made River Project, Libyan Arabjamahiriya IAEA-CN-151/63, 487–494, 2007.

Mittermayr, F., Bauer, C., Klammer, D., Böttcher, M. E., Leis, A., Escher, P., and Dietzel, M.: Concrete under Sulphate Attack: An Isotope Study on Sulphur Sources, Isotop. Environ. Health Studies, 48, 105–117, 2012.

Morin, S., Savarino, J., Frey, M. M., Yan, N., Bekki, S., Bottenheim, J. W., and Martins, J. M. F.: Tracing the origin and fate of NO_x in the Arctic atmosphere using stable isotopes in nitrate, Science, 322, 730–732, 2008.

Morin, S., Savarino, J., Frey, M. M., Domine, F., Jacobi, H. W., Kaleschke, L., and Martins, J. M. F.: Comprehensive isotopic composition of atmospheric nitrate in the Atlantic Ocean boundary layer from 65° S to 79° N, J. Geophys. Res., 114, D05303, doi:10.1029/2008JD010696, 2009.

Morrison, J., Brockwell, T., Merren, T., Fourel, F., and Phillips, A. M.: On-line high-precision stable hydrogen isotopic analyses on nanoliter water samples, Anal. Chem., 73, 3570–3575, 2001.

Nakagawa, F., Suzuki, A., Daita, S., Ohyama, T., Komatsu, D. D., and Tsunogai, U.: Tracing atmospheric nitrate in groundwater using triple oxygen isotopes: evaluation based on bottled drinking water, Biogeosciences, 10, 3547–3558, doi:10.5194/bg-10-3547-2013, 2013.

Nielsen, H.: Sulphur isotopes, in: Lectures in Isotope Geology, edited by: Jager, E. and Hunziher, J. C., Springer Verlag, Berlin, 283–312, 1979.

Parkhurst, D. L. and Appelo, C. A. J.: User‘s Guide to PHREEQC (Version 2), a Computer Program for Speciation, Batch-Reaction, One-Dimensional Transport, and Inverse Geochemical Calculations, Water-Resources Investigations US Geol. Sur., 312 pp., 1999.

Rimstidt, J. D.: Quartz solubility at low temperatures, Geochim. Cosmochim. Ac., 61, 2553–2558, 1997.

Rognon, P.: Late quaternary climatic reconstruction for the Maghreb (north Africa), Palaeogeogr. Palaeocl., 58, 11–34, 1987.

Saccon, P., Leis, A., Marca, A., Kaiser, J., Campisi, L., Böttcher, M. E., Savarino, J., Eisenhauer, A., Escher, P., and Erbland, J.: Multi-isotope approach for the identification and characterisation of multiple nitrate pollution sources in the Marano Lagoon (Italy), and parts of its catchment area, Appl. Geochem., 34, 75–89, 2013.

Sahli, N. I. M.: Water Quality in the Hasouna Wellfields, Western Jamahirya System, Great Man Made River Project (GMRP), Ph.D. thesis, University of Technology, Sydney, Australia, 658 pp., 2006.

Salem, O.: The great manmade river project: a partial solution to Libya‘s future water supply, Int. J. Water Resour. D., 8, 270–278, 1992.

Salem, O., Visser, J. H., Dray, M., and Gonfiantini, R.: Groundwater flow patterns in the western Libyan Arab Jamahiriya evaluated from isotopic data, IAEA-AG-158/12, 165–178, 1980.

Savarino, J.: Laboratory oxygen isotopic study of sulfur(iv) oxidation: origin of the mass-independent oxygen isotopic anomaly in atmospheric sulfates and sulfate mineral deposits on Earth, J. Geophys. Res.-Atmos., 105, 29079–29088, 2000.

Savarino, J., Kaiser, J., Morin, S., Sigman, D. M., and Thiemens, M. H.: Nitrogen and oxygen isotopic constraints on the origin of atmospheric nitrate in coastal Antarctica, Atmos. Chem. Phys., 7, 1925–1945, doi:10.5194/acp-7-1925-2007, 2007.

Sonntag, C., Klitzsch, E., Löhnert, E. P., El-Shazly, E. M., Münnich, K. O., Junghans, C., Thorweihe, U., Weistroffer, K., and Swailem, F. M.: Paleoclimatic information from deuterium and oxygen-18 in carbon-14 dated north Saharan groundwaters, IAEA-SM-228/28, 569–581, 1978.

Srdoč, D., Sliepčević, A., Obelić, B., Horvatinčić, N., Moser, H., and Stichler, W.: Isotope investigations as a tool for regional hydrogeological studies in the Libyan Arab Jamahiriya, IAEA-AG-158/11, 153–164, 1980.

Thiemens, M. H.: Atmospheric science: the mass-independent ozone isotope effect, Science, 293, p. 226, 2001.

Thiemens, M. H.: History and applications of mass-independent isotope effects, Annu. Rev. Earth Pl. Sc., 34, 217–262, 2006.

Tsunogai, U., Komatsu, D. D., Daita, S., Kazemi, G. A., Nakagawa, F., Noguchi, I., and Zhang, J.: Tracing the fate of atmospheric nitrate deposited onto a forest ecosystem in Eastern Asia using Δ^{17}O, Atmos. Chem. Phys., 10, 1809–1820, doi:10.5194/acp-10-1809-2010, 2010.

Tsunogai, U., Daita, S., Komatsu, D. D., Nakagawa, F., and Tanaka, A.: Quantifying nitrate dynamics in an oligotrophic lake using Δ^{17}O, Biogeosciences, 8, 687–702, doi:10.5194/bg-8-687-2011, 2011.

Turner, P. and Sherif, H.: A giant Triassic-Jurassic evaporitic basin on the Sharan platform, North Africa, in: Evaporites Through Space and Time, edited by: Schreiber, C., Lugli, S., and Babel, M., Geol. Society London, Spec. Publ., 285, 87–106, 2007.

Tyler, S. W., Chapman, J. B., Conrad, S., Hammermeister, D., Blout, D., Miller, J., Sully, M., and Ginanni, J.: Soil Water Flux on the Nevada Test Site: Temporal and Spatial Variations over the Last 120,000 Years, Water Resour. Res., 32, 1481–1499, 1996.

Walvoord, M. A., Phillips, F. M., Stonestrom, D. A., Evans, R. D., Hartsough, P. C., Newman, B. D., and Striegl, R. G.: A reservoir of nitrate beneath desert soils: Science, 302, 1021–1024, 2003.

Wehausen, R. and Brumsack, H.-J.: Cyclic variations in the chemical composition of eastern Mediterranean sediments: a key for understanding sapropel formation, Mar. Geol., 153, 161–176, 1999.

WHO: Guidelines for Drinking Water Quality, Recommendations world health organization, Geneva: World Health Organization, 2004.

Xue, D., Botte, J., De Baets, B., Accoe, F., Nestler, A., Taylor, P., Van Cleemput, O., Berglund, M., and Boeckx, P.: Present limitations and future prospects of stable isotope methods for nitrate source identification in surface- and groundwater, Water Res., 43, 1159–1170, 2009.

Zhang, Y. C., Slomp, C. P., Broers, H. P., Bostick, B., Passier, H. F., Bottcher, M. E., Omoregie, E. O., Lloyd, J. R., Polya, D. A., and Van Cappellen, P.: Isotopic and microbiological signatures of pyrite-driven denitrification in a sandy aquifer, Chem. Geol., 300, 123–132, 2012.

Zhang, Y.-C., Slomp, C., Van Cappellen, P, Boers, H. P., Passier, H. F., Boettcher, M. E., Omoregie, E. O., Lloyd, J. R., and Polya, D. A.: Denitrification coupled to pyrite oxidation in sandy aquifer: stable isotope and microbiological evgidence, in: Water-Rock-Interaction XIII. Proc. Internat. Conf. Water-Rock-Interaction, WRI 13, edited by: Birkle, P. and Torres-Alarado, I. S., Taylor and Francis, 975–978, 2010.